Axial behaviour of Concrete Filled Double Skinned Steel Tubular (CFDST) column with concrete imperfections

Arth J. Patel, Sharadkumar P. Purohit
Civil Engineering Department, Institute of Technology, Nirma University, Gujarat, India
arth.patel@nirmauni.ac.in, http://orcid.org/0000-0003-2633-399X
sharad.purohit@nirmauni.ac.in, http://orcid.org/0000-0002-2678-4320

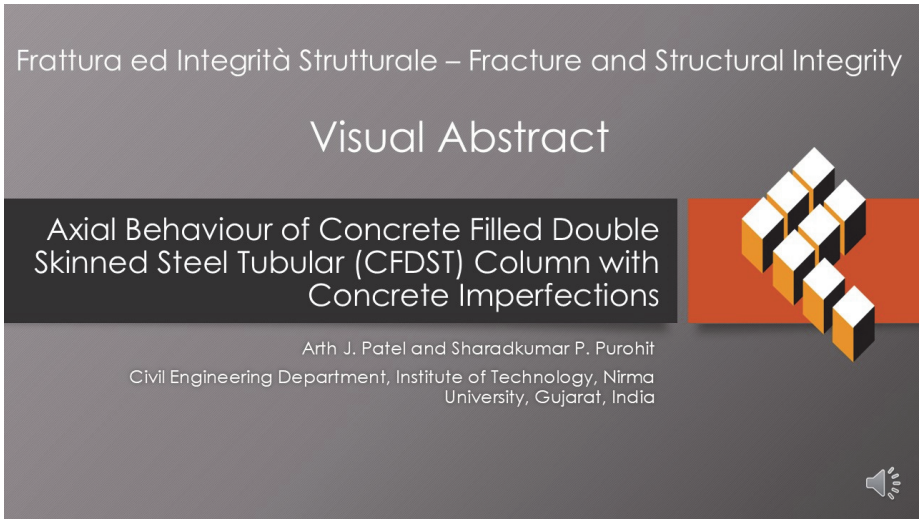

Citation: Patel, A. J., Purohit S. P., Axial behaviour of Concrete Filled Double Skinned Steel Tubular (CFDST) column with concrete imperfections, Fracture and Structural Integrity, 72 (2025) 1-14.

Received: 28.08.2024
Accepted: 13.12.2024
Published: 07.01.2025
Issue: 04.2025

KEYWORDS. Axial loading, Concrete imperfection, Confinement effect, Failure modes, Steel-concrete composite column.

INTRODUCTION

The Concrete Filled Double Skinned Steel Tubular (CFDST) composite columns are being widely adopted in high-rise buildings, bridges, and elevated corridors and are extensively being investigated under axial-flexural and torsional loading owing to their excellent load-carrying capacity, enhanced global stability, better strength to weight (s/w) ratio, superior ductility and convenience in construction [1–3]. Since two types of materials, Hollow Steel Tubes (HSTs) and concrete, are used to fabricate CFDST composite members, it is expected that there may be imperfections potentially originating from both the steel tube and sandwiched concrete commonly known as steel imperfection and concrete imperfection. Concrete imperfection is considered to be a serious issue as compared to steel imperfections as later being manufactured in controlled environments in industries. Concrete imperfection manifests due to improper construction practices, temperature gradient, shrinkage, creep, etc, and can be realized as gap defect as featured in Concrete Filled Steel Tube (CFST) members of arch bridges in China [4].
In the last two decades, most research studies reported in literature comprised experimental and/or numerical investigations on perfect (non-defective) CFDST composite columns under a variety of loadings [5–8]. However, gap defects may lead to very serious issues on the safety of composite columns owing to incorrect prediction of the ultimate load-carrying capacity

of the composite column as well as premature buckling of outer steel tube leading to brittle failure. Geometric imperfections can significantly reduce the strength of steel tubes and concrete cores by 14% as evident from experimental investigations [9]. Therefore, it becomes imperative to recognize the impact of gap defects on the composite column. The concrete imperfection gap ratio, χ is perceived as Circumferential Concrete Imperfections (CCI) and Spherical Concrete Imperfection (SCI) or Rectangular Concrete Imperfection (RCI) commonly encountered in composite columns, struts, and beam sections. [10]. The circumferential gap ratio of the CFDST member is defined as the ratio of circumferential gap (d_c) to the diameter or dimension (D_o) of outer steel tube as expressed by Eqn. 1. Analogously, spherical cap gap ratio as ratio of spherical cap gap (d_s) in circular CFDST or rectangular cap gap (d_r) in square CFDST to diameter or dimension (D_o) of outer steel tube represented by Eqn. 2.

$$\text{for CCI ratio: } \chi = \frac{2d_c}{D_o}\% \tag{1}$$

$$\text{for SCI ratio: } \chi = \frac{d_s \text{ or } d_r}{D_o}\% \tag{2}$$

Hu et. al. [11] indicated that up to the first peak load reached for CFST composite column of high-strength concrete with CCI imperfection, no composite interaction was visible due to less dilatancy characteristics of high-strength concrete as contrary to normal strength concrete. Hence, composite columns with high-strength concrete are vulnerable to use in case of a high circumferential gap ratio of ~1%. Square and rectangular CFST short columns with CCI showed up to 31% reduction in ultimate load-carrying capacity leading to an overestimation of composite columns [12]. The presence of multiple kinks while reaching the peak load and beyond in post-peak region reported during testing indicates the damage in the concrete. Liao et. al [10] carried out a series of compression and flexural tests to estimate the effect of circumferential gap and spherical cap gap on circular CFST composite column and recognized that circumferential gap significantly reduces the ultimate strength of specimen as compared to spherical cap gap. Shao et. al. [13] proposed limiting spherical cap gaps of 1.09% and 3.58% and circumferential gaps of 0.16% and 0.37% for circular and square shape CFST composite columns, respectively to ensure the safety of the column. Spherical cap gap in elliptical shaped CFST composite column had shown uneven damage of infilled concrete and inward buckling of steel tube thus, disturbing the longitudinal stress distribution that leads to the division of the infilled section into three parts namely; Fully Confined (FC) part, Partially-Confined (PC) part and Un-Confined (UC) part [14]. The discontinuity and interfacial behaviour of materials can be more precisely captured by extending an intriguing numerical technique employed by Siguerdjidjene et. al. [15]. Shen et. al. [16] tested elliptical-shaped CFST composite columns under eccentric compression loading and found that with the increase in eccentricity as well as spherical cap gap, the ultimate strength and ductility of test specimens reduced significantly.

The performance of CFST members with circumferential gap was tested under lateral impact and found almost the same type of behaviour regardless of concrete imperfection, though the local buckling and bending deflection were observed to be more significant with circumferential gap [17]. Wahrhaftig et. al. [18] studied an equivalent system of the slender column to evaluate strength and stability considering various parameters like cross-section, slenderness ratio, cracking formation and concrete creep. As the concrete core carries a significant load in steel-concrete composite columns, concrete imperfection significantly affects the load-carrying capacity of the test specimen. The casting of CFDST columns offers a challenge in both vertical and horizontal casting positions. While the in-situ vertical casting position of the column may lead to a circumferential gap as a result of shrinkage and creep, the horizontal casting position of column at the casting yard may result in a spherical cap gap on the top side of the column due to the settlement of lean concrete as a part of the construction process.

Substantial experimental studies are conducted on CFST composite columns including concrete imperfection, such studies are still missing for CFDST composite columns. The present study focuses on the experimental investigation of behaviour of CFDST composite column with concrete imperfection under axial compression as illustrated in the research framework in Fig. 1. There are currently no guidelines available in modern and well-established design codes that account for the effect of concrete imperfection on strength prediction. An effort has been made to close the knowledge gap regarding the prediction of strength of CFDST composite columns incorporating the effect of concrete imperfections. This paper includes the experimental study on total of 14 nos. of CFDST columns of outer circular and square steel tube and inner square steel tube with circumferential gap ratios (1.1% and 2.2%) and spherical cap gap ratios (4.4% and 8.8%). CFDST Columns were tested under axial compression loading and the behaviour was evaluated in terms of ultimate strength, ductility, failure mode, confinement, and strain distribution profile. New strength reduction factors, η_r are proposed to accurately predict the

strength of CFDST composite columns with concrete imperfections, based on the experimental test results and predicted results determined following the modified strength equation of European code, EC-4 [19] presented in the early study [20].

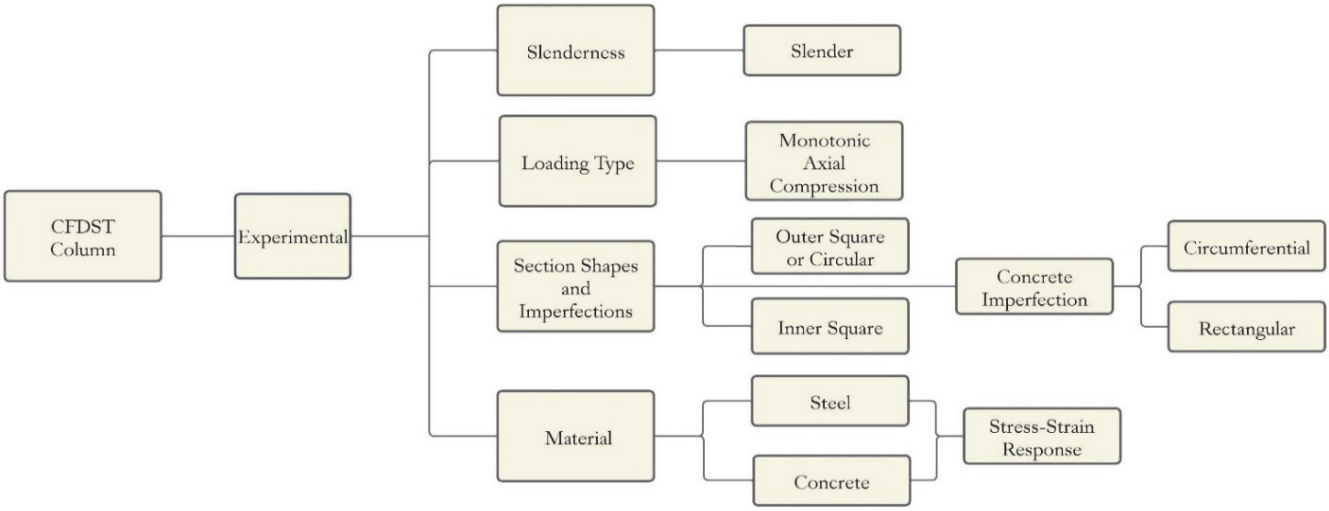

Figure 1: Research framework of the present study.

EXPERIMENTAL PROGRAM

A detailed experimental program including specimen details and preparation, mechanical properties of constituent materials of CFDST composite column, instrumentation, and test procedure were developed and discussed in the following sub-sections.

Specimens details and preparation

CFDST column test specimens of circumferential concrete imperfection (02 nos.), spherical or rectangular concrete imperfection (02 nos.) and without concrete imperfection (01 nos.) for each circular and square shape outer steel tube and square shape inner steel tube were fabricated as depicted in Fig. 2. For comparison, CFST columns and HST columns of circular and square shape were also prepared to study the efficacy of corresponding CFDST columns. Specimen ID was assigned to each test specimen comprising notation where the first and second letter pertaining to the shape of the outer and inner steel tubes (circular or square), respectively followed by column type (CFDST or CFST or HST) and the last term represents the type of concrete imperfection (CCI or SCI), if any.

The geometrical properties of all column test specimens are tabulated in Tab. 1 and experimentally obtained strength are also presented. The cross-sectional area of the steel tubes for all columns is kept approximately same for benchmarking and comparison. The hollow steel tubes of Y_{st} 310 grade, from APL APOLLO company, were procured and were cut into pieces 750 mm length using the metal cutter. Firstly, the top and bottom end surfaces of HSTs were faced on the lathe machine for levelling. The end platens of 110 mm × 110 mm × 20 mm size were grooved for 25 mm wide and 4 mm deep size with a vertical ball mill cutter to accommodate rigid roller to transfer vertical load on CFDST column through hinged end condition. In case of CFDST and CFST column test specimens, the bottom ends of tubes were welded to bottom end platens and subsequently filled with normal strength Self Compacting Concrete (SCC). The exposed top surfaces of CFDST and CFST column test specimens were surface cured for 28 days before welding the top-end platen. For the HST columns, both ends were welded with non-grooved end platens to test under fixed boundary conditions since with pinned condition it failed by end brooming as observed in pilot studies. All columns were cast in a vertical position with special formwork to induce concrete imperfection. Oiled PVC sheets of 0.5 mm, 1 mm thickness were placed inside the outer steel tube throughout the length before pouring the concrete and were stretched from the top to slide after the required initial setting of concrete to create a circumferential concrete gap in circular and square shape. A spherical or rectangular concrete imperfection in circular and square-shaped CFDST columns, respectively was induced by placing PVC mould of the required shape and size, which was pulled out by a sliding mechanism. Care has been taken that SCI or RCI cap gap induces at Face ‘ B ’ of each corresponding test specimen to make them comparable as shown in Fig. 4.

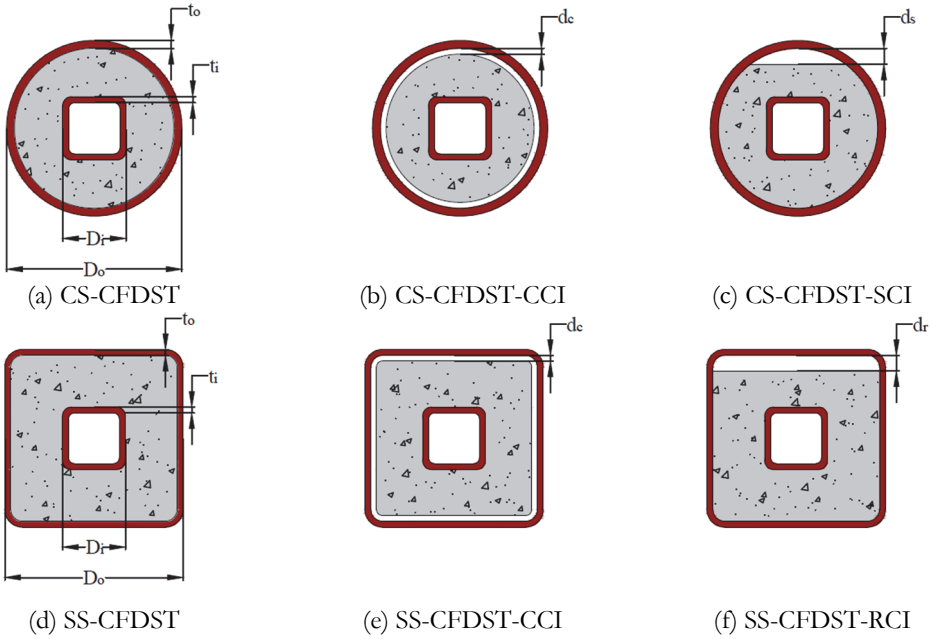

(a) CS-CFDST (b) CS-CFDST-CCI (c) CS-CFDST-SCI

(d) SS-CFDST (e) SS-CFDST-CCI (f) SS-CFDST-RCI

Figure 2: Cross-sectional denotation of CFDST composite column with and without concrete imperfection.

Specimen ID	Outer Steel Tube			Inner Steel Tube			$\alpha = A_a/A_c$	d_c or d_s (mm)	χ (%)	$N_{u,exp}$ (kN)	s/w
	D_o (mm)	D_o/t_o	A_{ao} (mm^2)	D_i (mm)	D_i/t_i	A_{ai} (mm^2)					
CS-CFDST	90	22.23	1063	32	10.70	348	0.34	-	-	667	41.52
CS-CFDST-CCI1	90	22.23	1063	32	10.70	348	0.36	0.5	1.1	609	39.02
CS-CFDST-CCI2	90	22.23	1063	32	10.70	348	0.39	1.0	2.2	599	39.51
CS-CFDST-SCI4	90	22.23	1063	32	10.70	348	0.35	4.0	4.4	621	39.07
CS-CFDST-SCI8	90	22.23	1063	32	10.70	348	0.37	8.0	8.8	590	37.85
SS-CFDST	91	30.33	1056	32	10.70	348	0.23	-	-	664	34.12
SS-CFDST-CCI1	91	30.33	1056	32	10.70	348	0.27	0.5	1.1	565	31.78
SS-CFDST-CCI2	91	30.33	1056	32	10.70	348	0.29	1.0	2.2	541	31.55
SS-CFDST-SCI4	91	30.33	1056	32	10.70	348	0.27	4.0	4.4	629	35.39
SS-CFDST-SCI8	91	30.33	1056	32	10.70	348	0.29	8.0	8.8	557	32.54
C-CFST	90	22.23	1063	-	-	-	0.21	-	-	575	36.85
S-CFST	91	30.33	1056	-	-	-	0.15	-	-	520	27.00
C-HST	90	22.23	1063	-	-	-	-	-	-	349	54.89
S-HST	91	30.33	1056	-	-	-	-	-	-	316	50.54

D_o, t_o, A_{ao} = diameter or dimension, thickness, area of outer steel tube, respectively; D_i, t_i, A_{ai} = depth or dimension, thickness, area of inner steel tube, respectively; A_a is total steel tube area and A_c is effective concrete area.

Table 1: Geometrical properties of column test specimens.

Mechanical properties of constituent materials

Self-compacting concrete with average characteristic compressive strength (cube), $f_{ck,avg}$ of 27.5 MPa and modulus of elasticity, $E_{c,avg}$ of 25797 MPa was evaluated following IS 516: 2021 [21] and was used as infill for CFDST and CFST column test specimens. The concrete mix design was carried out as per IS 10262: 2019 [22] and is given in Tab. 2. Tension tests on coupons extracted from two faces of circular and square shaped hollow steel tubes each were performed following the IS 1608: 2005 [23] as shown in Fig. 3(a). An extensometer (Epsilon) of 15 mm stroke length and 50 mm gauge length

was attached over the coupon to measure the longitudinal strain as depicted in Fig. 3(b). Real-time data of load and strain were recorded for each coupon to develop engineering stress, f and strain, ε relationship including yield loads and non-linear behaviour as represented by sample $f-\varepsilon$ curves shown in Fig. 3(c). The mechanical properties i.e., yield stress (f_a), yield strain (ε_a), ultimate stress (f_u), ultimate strain (ε_u), and modulus of elasticity (E_a) of the sample coupons corresponding to C-HST and S-HST are summarized in Tab. 3.

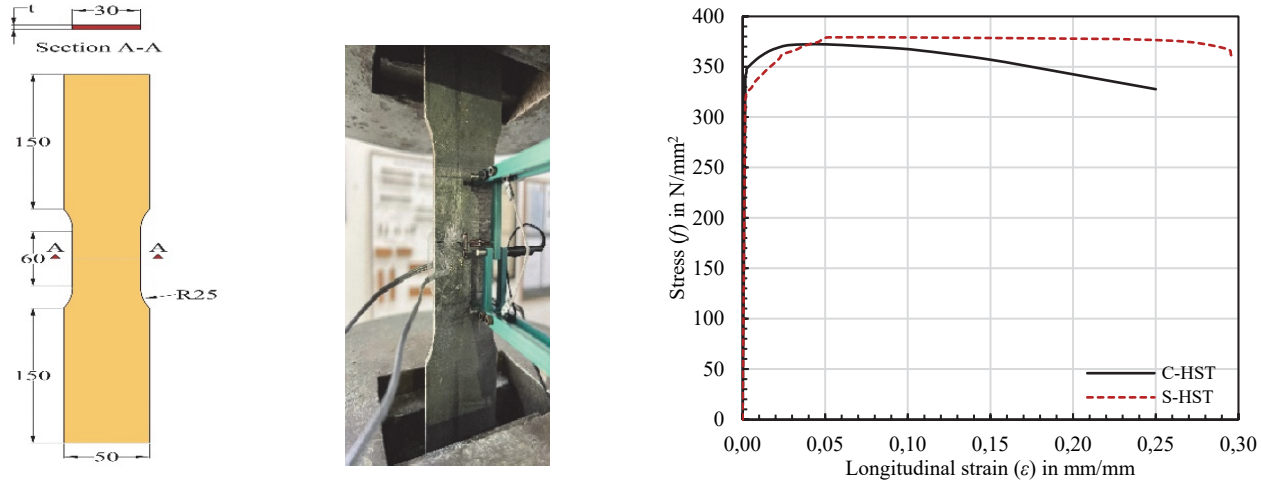

(a) Details of coupon (b) Test set-up and instrumentation (c) Sample stress-strain curve of steel coupon

Figure 3: Tension test of steel coupons.

Cement (kg/m³)	Water (Lt/m³)	Sand (kg/m³)	Aggregate (kg/m³)	Superplasticiser (kg/m³)	$f_{ck,avg}$ (MPa)	$E_{c,avg}$ (MPa)
444.44	213.33	944.44	781.14	2.67	27.5	25797

Table 2: Mix-Design of self-compacting concrete.

Coupon ID	Width, b_{avg} (mm)	Thickness, t_{avg} (mm)	Yield Stress, f_a (MPa)	Yield Strain, ε_a	Ultimate Stress, f_u (MPa)	Ultimate Strain, ε_u	Modulus of Elasticity, E_a (MPa)
C-HST	29.96	3.71	341.22	0.0024	372.16	0.0512	197200
S-HST	30.01	3.01	320.83	0.0019	379.17	0.0516	195500

Table 3: Average geometrical and mechanical properties of steel coupons.

Instrumentation and test procedure

An effective loading mechanism, utilizing the full length of the column test specimen, has been developed for testing CFDST and CFST column test specimens as shown in Fig. 4 (a) [24,25]. The HST column test specimens were tested under fixed-end conditions to avoid local brooming failure. Each column test specimen was instrumented with strain gauges, and load-displacement sensors to measure important physical quantities. A multi-channel data acquisition system (Data Taker DT-80) was used to capture real-time data during the testing and were processed with a high-end computer system. Upto 16 nos. of strain gauges were attached on three faces i.e. (Face ' B ', Face ' C ', and Face ' D ') along three sections i.e. C-C (mid-height), T-T (100 mm from top end), and B-B (100 mm from bottom end) of each column test specimen as shown in Fig. 4(b) to capture the variation of strain along the length as well as on different faces of the column. Two Linear Variable Differential Transducers (LVDTs) were placed on opposite faces (i.e. Face ' B ' and Face ' D ') of the column test specimens to monitor mid-height lateral displacement and one LVDT was placed along the length of the column test specimens to measure axial deformation. Ultimate load carrying capacity, axial and lateral displacements as well as longitudinal and lateral strains were extracted for each column test specimen considered in the present study. Composite column test specimens were tested under axial compression load through the loading frame of 1000 kN capacity. The experiment was continued

for each column test specimen up to the ultimate load, $N_{u,exp}$, and beyond until post-peak load reaches $0.4N_{u,exp}$ or apparent large deformation observed.

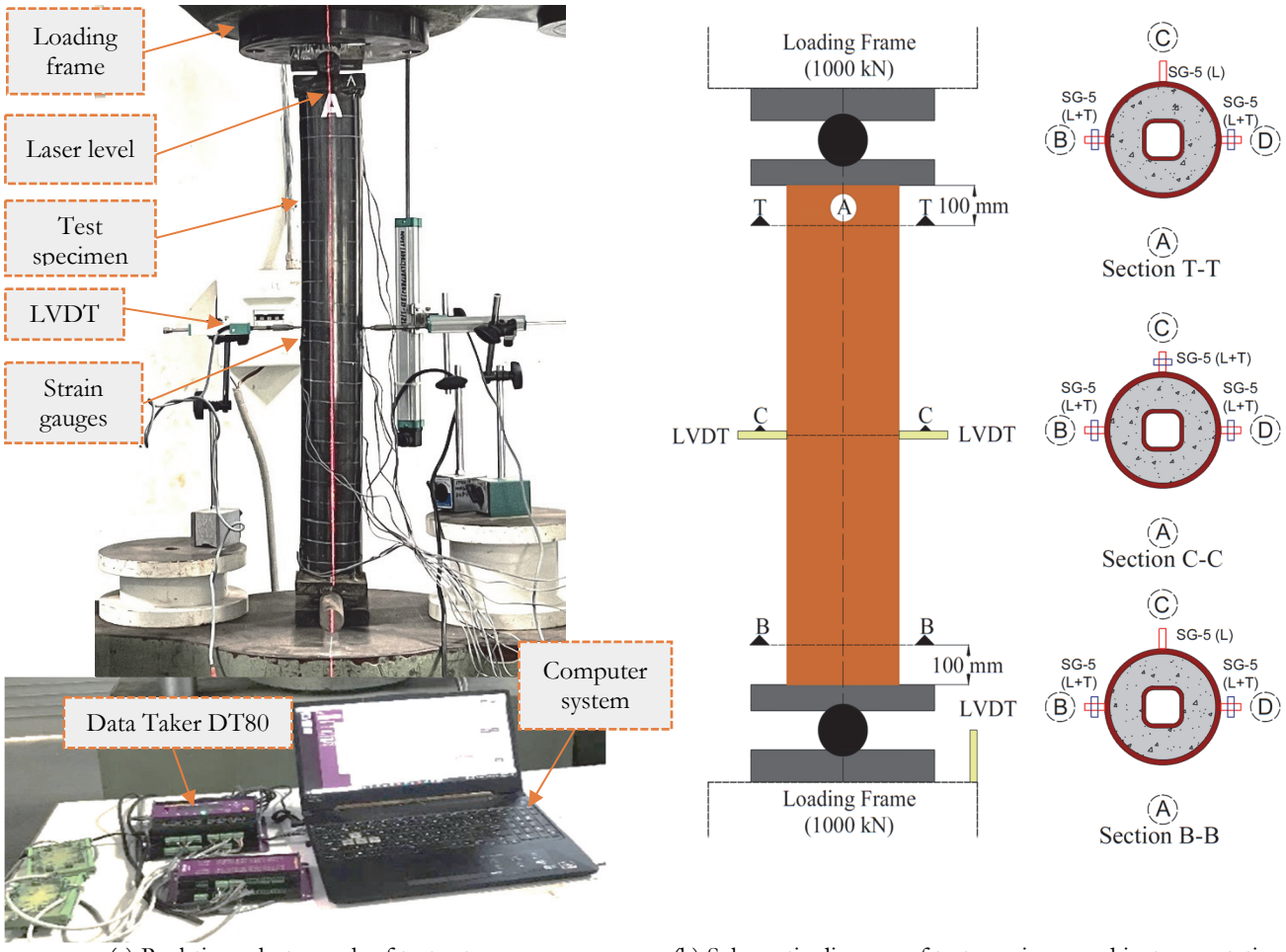

(a) Real-time photograph of test set-up (b) Schematic diagram of test specimen and instrumentation

Figure 4: Column test set-up and instrumentation.

EXPERIMENTAL RESULTS AND DISCUSSION

Ultimate load carrying capacity

The effect of concrete imperfection on ultimate load carrying capacity, $N_{u,exp}$ of circular and square shaped CFDST composite columns was examined and plotted with a bar chart in Fig. 5. It is evident that the circumferential gap significantly reduces the strength of columns as compared to spherical or rectangular cap gap defect in both CS-CFDST and SS-CFDST columns. The circumferential concrete imperfection gap ratios of 1.1% and 2.2% in CS-CFDST columns exhibit a strength reduction of approximately 9% and 10%, respectively, and approximately 15% and 19% strength reduction in the case of SS-CFDST columns. A higher reduction in square-shaped CFDST composite columns proves that the absence of composite action between steel and concrete may lead to local plate bending of outer square tube and accelerate premature buckling. Hence in the square-shaped CFDST, circumferential concrete imperfection should be avoided. Composite action in test specimens with spherical or rectangular concrete imperfection defect is compromised for a small part of the section hence less amount of reduction in strength can be seen. Test results of CS-CFDST columns show a strength reduction of ~7% for a 4.4 % spherical cap gap ratio and ~12% for an 8.8 % spherical cap gap ratio. Whereas, ~5% and 16% strength reduction are observed for SS-CFDST columns with 4.4% and 8.8% rectangular cap gap ratios, respectively. Approximately 13% and 22% higher strength for CS-CFDST and SS-CFDST columns, respectively were observed as compared to their counterpart CFST columns.

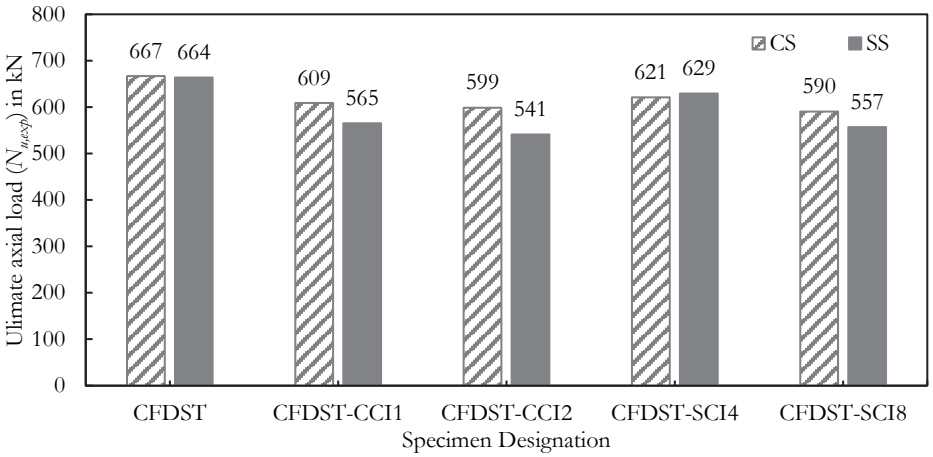

Figure 5: Experimental ultimate load-carrying capacity of CFDST columns.

Load-Displacement behaviour ($N - \Delta$) and ductility

Axial load-displacement ($N - \Delta$)curves were plotted for CS-CFDST and SS-CFDST columns in Fig. 6(a) and Fig. 6(b), respectively. CS-CFDST columns exhibit steep stiffness degradation of the axial load-displacement curve in the post-peak region with an increase in circumferential gap ratio. This is attributed to the global buckling behaviour of CS-CFDST column test specimens. It can further be realized that stiffness degradation is higher for CS-CFDST column test specimens with concrete imperfection since imperfection affects the composite action. Axial load-displacement curves of square-shaped CFDST columns shown in Fig. 6(b) depict many humps indicating the presence of multiple local buckling and strain hardening following each local buckling until the testing stopped. It can be realized that in case of concrete imperfection, the inner steel tube stabilizes post-peak ultimate axial load behaviour and prevents premature buckling up to a certain extent. Inelastic axial displacement behaviour further gets strengthened because of the inner steel tube since sandwiched concrete may yield uniform confinement in addition to the delayed local buckling.

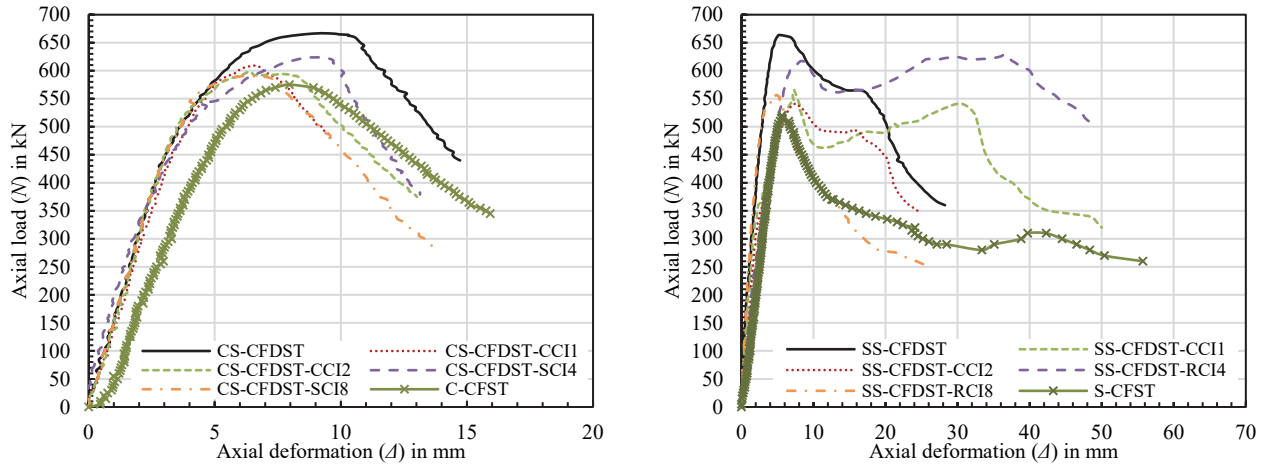

Figure 6: Axial load versus axial displacement behaviour of columns (a) CS-CFDST; (b) SS-CFDST.

Ductility of each CS-CFDST and SS-CFDST column was evaluated through the Ductility Index (*DI*) as listed in Tab. 4. *DI* is defined as a ratio of axial shortening, $\Delta_{u,85\%}$ corresponding to the axial load once the peak load falls by 15% and axial shortening, Δ_u corresponding to peak axial load as represented by Eqn. 3 [26].

$$DI = \frac{\Delta_{u,85\%}}{\Delta_u} \tag{3}$$

It is evident from Tab. 4 that SS-CFDST columns yield substantially higher *DI* vis-à-vis CS-CFDST, C-CFST, and S-CFST columns. The increase in circumferential gap defect led to a significant reduction of ductility for SS-CFDST columns as compared to CS-CFDST columns. It was observed that the reduction in *DI* of SS-CFDST column with circumferential gap defect is higher vis-à-vis rectangular cap gap defect since the former has no confinement contribution. CS-CFDST columns with circumferential and spherical cap gap defects yield a relatively small reduction in *DI* owing to global buckling.

Damage and failure mechanism

Column test specimens with outer circular steel tubes i.e. CS-CFDST, C-CFST show global buckling failure mechanism in general, as demonstrated in Fig. 7(a) to Fig. 7(f), whereas SS-CFDST and S-CFST columns show local bucking (multiple) near either of the ends as depicted in Fig. 7(g) to Fig. 7(l). Separation of the outer steel tube from sandwiched concrete was distinctly visible from the failure modes of all CFDST columns although it was prominent for test specimens with spherical or rectangular cap gap defects. Both CS-CFDST and SS-CFDST columns with CCI show premature local inward plate bending of the outer steel tube near the top and bottom ends in the early stage of axial compression loading. CS-CFDST columns with SCI suffer from local tube buckling on the side of the gap defect. SS-CFDST columns with RCI show local buckling initiated on the face of the gap defect (i.e. Face ' B ') and subsequently propagated to the whole cross-section as shown in Fig. 7(j) and Fig. 7(k). SS-CFDST column with a small RCI gap ratio (i.e. 4.4%) shows crushing of concrete and filling up of gap on attaining the peak load and thus, reattaining the strength before elephant foot type buckling initiated at the bottom end as contrary to sudden failure in case of test specimen with 8.8% RCI gap ratio. Hence, such type of concrete imperfections should be avoided by following proper construction practices. Failure of S-CFST column shows strain hardening after reaching the ultimate load against to C-CFST column. It is interesting to note that C-CFST showed a fracture of the outer steel tube after crushing of concrete accompanied by noise at mid-height at 40% of post-peak load.

(a) CS-CFDST (b) CS-CFDST-CCI1 (c) CS-CFDST-CCI2 (d) CS-CFDST-RCI4 (e) CS-CFDST-RCI8 (f) C-CFST

(g) SS-CFDST (h) SS-CFDST-CCI1 (i) SS-CFDST-CCI2 (j) SS-CFDST-RCI4 (k) SS-CFDST-RCI8 (l) S-CFST

Figure 7: Failure modes of composite columns.

Strain analysis and confinement mechanics

Longitudinal strain, ε_L and transverse (hoop) strain, ε_T results were determined for CFDST and CFST columns to understand composite action amongst steel tubes and sandwiched concrete. The impact of confinement of sandwiched concrete due to the presence of concrete imperfection was evaluated from these results. Fig. 8(a) and Fig. 8(b) represent longitudinal strain measured on the outer steel tube for CS-CFDST and SS-CFDST columns, respectively. It is evident from Fig. 8(a) that CS-CFDST column shows uniform load distribution on opposite faces ' B ' and ' D ' of the test specimen indicating a proper bond between sandwiched concrete and steel tubes and the presence of composite action. Global buckling of the CS-CFDST column yields uniform tensile strain up to its ultimate strain value of ~0.05 while compressive strains are non-uniform and undergo larger strain, beyond ultimate strain under tension as specified by Fig. 8(a). It can be seen that CS-CFDST column test specimens with concrete imperfection yield lower peak axial load and longitudinal strain at every loading stage as compared to CS-CFDST column test specimens, except CS-CFDST-CCI1 specimen. It further reveals that Face ' B ' of CS-CFDST column test specimens with concrete imperfection; circumferential and spherical shows global buckling and thus, undergoes large strain on compression face due to buckling while the strain on tension face, Face ' D ' was lower for each CS-CFDST column test specimens with concrete imperfection. With the increase in concrete imperfection gap ratio; circumferential and spherical further reduce peak axial load and longitudinal strain. Compression of CS-CFDST column test specimens with circumferential and spherical defects; CS-CCI1 yields lower peak load and low longitudinal strain vis-à-vis CS-CFDST and SS-CFDST column test specimen under axial compression loading that further reduces for CS-CCI2 and CS-SCI8 where later is the least and thus showing no confinement effect.

The longitudinal strain measured for all SS-CFDST column test specimens is plotted in Fig. 8(b). It is evident that the SS-CFDST column test specimen yields a higher peak load and longitudinal strain. The faces of SS-CFDST column test specimens yield plate bending from the initial stages of the axial loading resulting in to increase in longitudinal strain, unlike CS-CFDST column test specimen. It can further be seen that the longitudinal strain measured was higher on the compression face of the test specimens with circumferential and rectangular gap concrete defects due to local buckling towards top end of the column test specimens. Like with CS-CFDST specimens with concrete defects, peak axial load, and longitudinal strain reduce for SS-CFDST column test specimens with the increase in concrete imperfection ratios. It was observed that the rectangular gap type of concrete defect yields higher peak axial load and longitudinal strain as compared to SS-CFDST test specimens with circumferential gap defects.

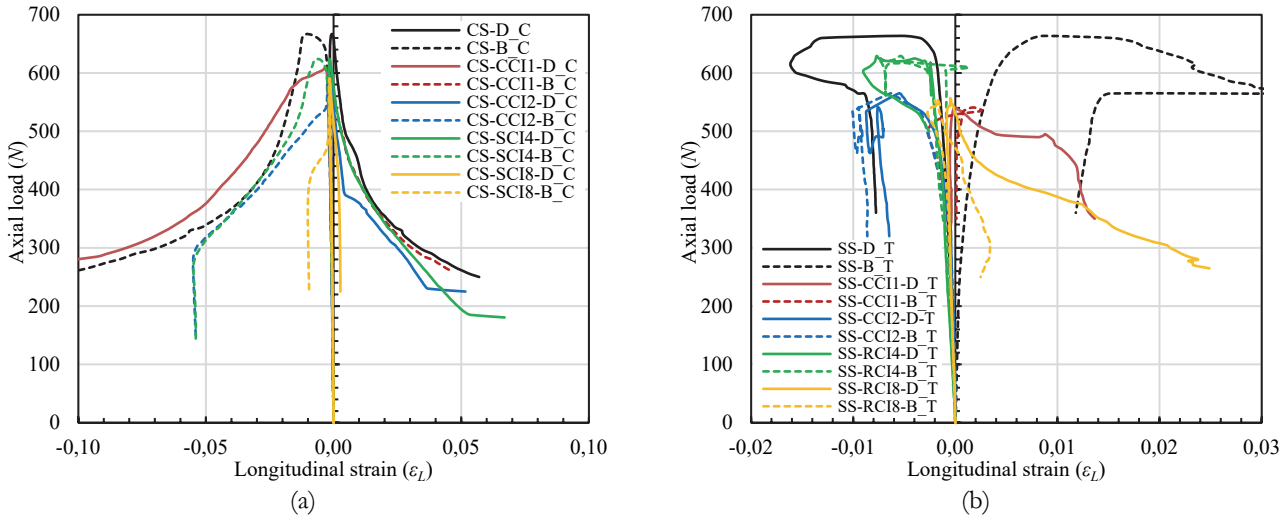

Figure 8: Axial load versus longitudinal strain behaviour (a) CS-CFDST; (b) SS-CFDST.

Normalized axial load versus transverse strain (ε_T) to longitudinal strain (ε_L) measured along the height (centre and near the top end) for CS-CFDST and SS-CFDST column test specimens are plotted in Fig. 9 and Fig. 10, respectively to capture confinement of sandwiched concrete with and without concrete imperfection. CS-CFDST column test specimen shows prominent confinement of concrete on reaching the peak axial load at the centre of the test specimen, while SS-CFDST column yields significant confinement of concrete at an axial loading level of ~40-60% of the axial load near top end support. However, strain ratios near the end support of CS-CFDST columns are observed with deviation at an axial load level of ~80% of the peak axial load, despite initial data being erratic due to unknown reasons. It is evident from Fig. 9(a) that CS-CFDST column test specimens with circumferential concrete imperfection, i.e., CCI1 and CCI2 show negligible

deviation in strain ratio up to peak axial load indicating the absence of any confinement at the centre of the specimen and thus, no composite action which was expected since outer steel tube and sandwiched concrete don't have any bond.

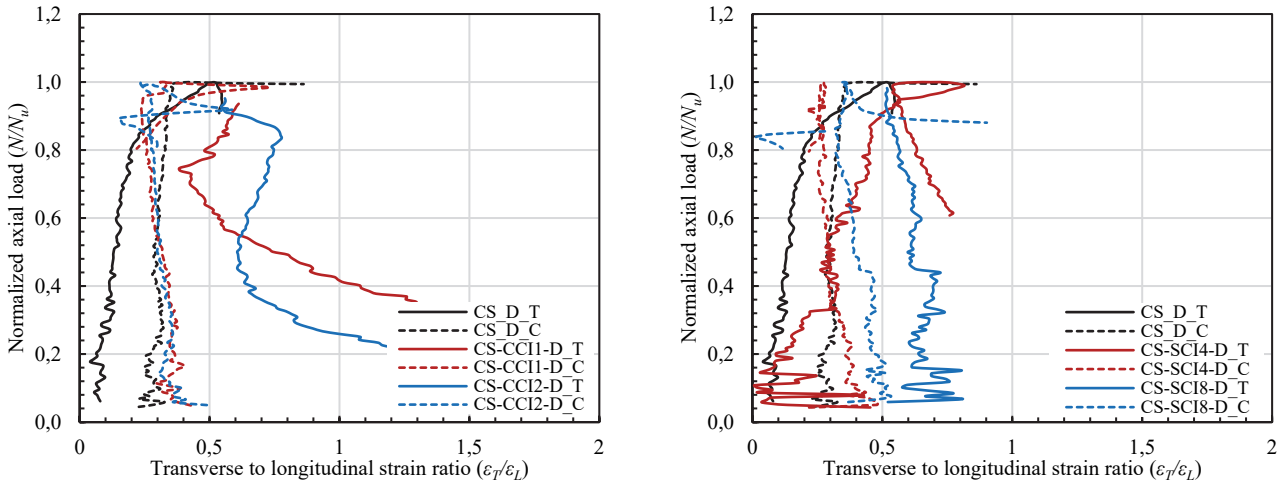

(a) Circumferential concrete imperfection (b) Spherical concrete imperfection

Figure 9: Normalized axial load to strain ratio for CS-CFDST columns along the length.

It can be observed from Fig. 9(b) that CS-CFDST column test specimens with spherical concrete imperfection exhibit no confinement for sandwiched concrete except CFDST column with spherical cap gap ratio 4.4% (i.e. SCI4) that shows a deviation in strain ratio at axial loading level ~40-60% of the peak axial load near the end support. For SS-CFDST column test specimen without concrete imperfection, confinement of concrete is observed at an early stage of axial loading ~40% of the peak axial load near the end of the specimen but no confinement is visible at the centre of the test specimen since SS-CFDST specimen undergoes local buckling near the end of the specimen. A similar observation can be made for SS-CFDST column test specimens with circumferential concrete imperfection since the strain ratio shows prominent deviation at axial loading level ~40% and 80% of the peak axial load for test specimens with 1.1% and 2.2% of CCI, respectively near the end of the test specimens owing to local buckling of these test specimen unlike to deviation in strain ratio at centre of the test specimen. SS-CFDST column test specimens with rectangular gap imperfections exhibit confinement of concrete at axial loading level ~40% of peak axial load near the end support of these test specimens similar to SS-CFDST with circumferential concrete imperfections. SS-CFDST specimens show no strain ratio deviation at the centre of the specimen indicating the absence of confinement effect for the specimens.

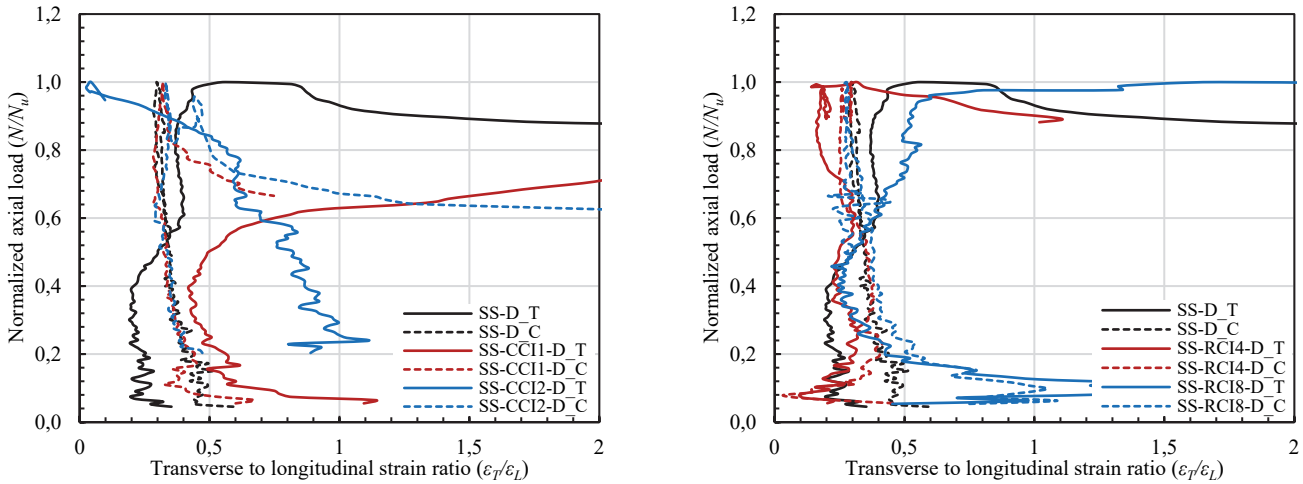

(a) Circumferential concrete imperfection (b) Rectangular concrete imperfection

Figure 10: Normalized axial load to strain ratio for SS-CFDST columns along the length.

Prediction model and strength reduction factor

The peak axial load carrying capacity, $N_{u,ana}$ of each CFDST column is predicted using the modified EC-4 equation proposed by Pagoulatou et. al. [20] as presented with Eqn. 4, assuming that the outer steel tube served as the primary means of confinement to the sandwiched concrete. Confinement coefficients, η_a and η_c corresponding to steel and concrete, respectively as presented in Eqn. 4, were taken into account solely to predict the capacity of CS-CFDST column. They are eliminated for SS-CFDST columns following EC-4 recommendation for square-shaped CFST columns and also for CS-CFDST with concrete imperfections. Peak axial load ratio, $N_{u,ana}/N_{u,exp}$ are evaluated for all CFDST columns and are tabulated in Tab 4. It shows an underestimation of up to about 11%, when comparing the experimental and predicted peak loads of CS-CFDST and SS-CFDST composite column. Therefore, it is believed that these confinement coefficients are insufficient for the CS-CFDST column and there is an existence of confinement in SS-CFDST column as well. Hence SS-CFDST column was re-assessed with set of equations proposed by Han et. al. [27] and the result showed a more accurate prediction of peak load with a variance of less than ~1%. Although it is evident that peak axial load estimated using Eqn. 4 for CS-CFDST and SS-CFDST columns with circumferential gap ratio of 1.1% and 2.2% and spherical or rectangular cap gap ratio of 4.4% and 8.8% yield close agreement with experimental results.

$$N_{u,ana} = \eta_a(A_{ao} \times f_{ao} + A_{ai} \times f_{ai}) + A_c \times f_c\left(1 + \eta_c \frac{t_o}{D_o}\frac{f_{ao}}{f_c}\right) \quad (4)$$

Here, f_{ao} is yield strength of outer steel tube, f_{ai} is yield strength of inner steel tube, f_c is compressive strength of concrete (cylinder).

Specimen ID	χ (%)	$N_{u,exp}$ (kN)	$N_{u,ana}$ (kN)	DI	SI	$N_{u,ana}/N_{u,exp}$
CS-CFDST	-	667	596	1.32	-	0.89
CS-CFDST-CCI1	1.1	609	589	1.30	0.91	0.97
CS-CFDST-CCI2	2.2	599	583	1.25	0.90	0.97
CS-CFDST-SCI4	4.4	621	594	1.21	0.93	0.96
CS-CFDST-SCI8	8.8	590	589	1.37	0.89	1.00
SS-CFDST	-	664	591	3.19	-	0.89
SS-CFDST-CCI1	1.1	565	582	2.61	0.85	1.03
SS-CFDST-CCI2	2.2	541	574	1.29	0.82	1.06
SS-CFDST-SCI4	4.4	629	573	1.57	0.95	0.91
SS-CFDST-SCI8	8.8	557	556	1.45	0.84	1.00
C-CFST	-	575	555	1.44	-	0.97
S-CFST	-	520	481	1.55	-	0.93

Table 4: Experimental and analytical results for CFDST and CFST columns.

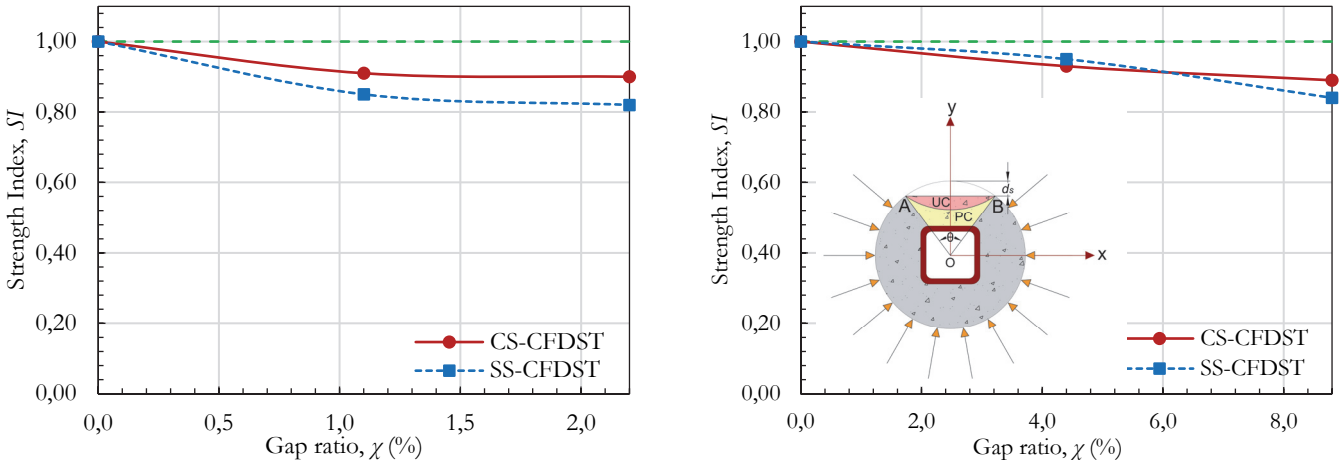

(a) CCI gap ratio (b) SCI or RCI gap ratio

Figure 11: Strength Index versus gap ratio for CS-CFDST and SS-CFDST.

For insight into the impact of concrete imperfection on peak axial load carrying capacity of CFDST columns with concrete imperfections, a Strength Index (*SI*) is defined as the ratio of the peak axial load of CFDST column with concrete imperfection to peak axial load of CFDST column without concrete imperfection are evaluated and summarised in Tab. 4. It is evident that *SI* shows decrement with an increase in concrete imperfection ratios for CS-CFDST and SS-CFDST columns. Fig. 11(a) and Fig. 11(b) show the strength index plotted against the concrete imperfection gap ratio, χ for CCI and SCI or RCI, respectively for both CS-CFDST and SS-CFDST columns. Lastly, new strength reduction factors, η_r are proposed to estimate reduced peak axial load capacity, $N_{u,CI}$ of CS-CFDST and SS-CFDST columns with circumferential and/or spherical or rectangular concrete imperfections, respectively accounting for the influence of concrete imperfection gap ratio, χ. In the absence of code provisions, proposed Eqn. 5 can effectively be utilized to estimate the peak axial load capacity of CFDST columns with concrete imperfections based on accurately predicted strength of non-defective CFDST columns as follows.

$$N_{u,CI} = \eta_r \, N_{u,ana} \tag{5}$$

Based on the decreasing trend seen in Figures 11(a) and 11(b), strength reduction factors, η_r can be calculated for each gap ratio (χ) of each CS-CFDST and SS-CFDST column as follows.

a) CFDST column with CCI

$$\eta_r = 1 - 0.1182\chi + 0.0331\chi^2 \; (\chi \leq 2.2) \tag{6}$$

$$\eta_r = 0.9 \; (\chi > 2.2) \tag{7}$$

for CS-CFDST

$$\eta_r = 1 - 0.1909\chi + 0.0496\chi^2 \; (\chi \leq 2.2) \tag{8}$$

$$\eta_r = 0.8 \; (\chi > 2.2) \tag{9}$$

for SS-CFDST

b) CFDST column with SCI/RCI

$$\eta_r = 1 - 0.0193\chi \quad \text{for CS-CFDST} \tag{10}$$

$$\eta_r = 1 - 0.0045\chi \quad \text{for SS-CFDST} \tag{11}$$

The proposed equation is more reasonable and is in good agreement with the experimental capacities of CFDST columns with concrete imperfections. In order to precisely quantify the un-confined and partially-confined area at the location of the spherical or rectangular cap gap for the CFDST column section and evaluate the proposed strength reduction factor, the present study can be further investigated with more finite element analysis and experimental investigations. An attempt was made to ascertain the un-confined and partially-confined area for spherical concrete imperfection in the CS-CFDST section, assuming a depth of un-confined region comparable to that of a spherical cap gap depth, d_s with the following equations. (Refer Fig. 11(b)).

Angle (AOB), θ in radian comprising the spherical cap gap defect is given by

$$\theta = 2cos^{-1}\left(1 - \frac{d_s}{r_c}\right) \tag{12}$$

Area of confined concrete, $A_{c,cc}$ in mm^2 is calculated as follows

$$A_{c,cc} = A_c - {r_c}^2(\theta - sin\theta) \tag{13}$$

Area of un-confined concrete, $A_{c,uc}$ in mm^2 is calculated as follows:

$$A_{c,uc} = 0.5{r_c}^2(\theta - sin\theta) \tag{14}$$

Area of partially-confined concrete, $A_{c,pc}$ in mm² is calculated as follows:

$$A_{c,pc} = 0.5{r_c}^2 sin\theta - 0.25{D_i}^2 tan(0.5\theta) - A_{c,uc} \quad (15)$$

where, r_c represents radius of concrete (OA or OB) in mm.

CONCLUSIONS

Impact of concrete imperfection in terms of circumferential gap ratio (1.1% and 2.2%) and spherical or rectangular cap gap ratio (4.4% and 8.8%) on axial strength of CFDST column with outer circular and square steel tubes and inner square steel tubes are studied experimentally. Comparison of strength is also carried out with CS-CFDST and SS-CFDST columns without concrete imperfection as well as C-CFST and S-CFST columns. In addition to the axial strength of CFDST columns, performance parameters related to axial behaviour like axial displacement, ductility, confinement effect, strain profile and failure modes are studied. New strength reduction factors, η_r are proposed to accurately predict the strength of CFDST composite columns with concrete imperfections, based on the experimental test results and results predicted following the modified strength equation of European code, EC-4 [19] presented in the early study [20]. The following critical observations are made from the present study.

- CFDST columns with circumferential and spherical or rectangular gap imperfections yield moderate reduction in the axial strength vis-à-vis CFDST columns without any concrete imperfection. Circumferential gap imperfections of CFDST columns exhibit a higher reduction in axial strength as compared to spherical or rectangular gap imperfections.
- The ductility of CFDST column test specimens was found to decrease with an increase in both types of concrete imperfections (i.e. circumferential and spherical or rectangular). However, SS-CFDST columns yield relatively higher ductility as compared to CS-CFDST columns owing to multiple local buckling near top-end support.
- Failure modes of CFDST sections with various concrete imperfections revealed global buckling in the case of CS-CFDST columns and local buckling for SS-CFDST columns.
- Axial load to longitudinal strain relationship of CS-CFDST and SS-CFDST columns with concrete imperfections demonstrate higher strain on compression face resulting from the confinement of concrete at higher axial loading level (~60-80%). However, the confinement effect for these specimens diminishes with an increase in concrete imperfection gap ratios.
- Proposed strength reduction factors, η_r for CS-CFDST and SS-CFDST columns based on experimental studies provide a good estimation of axial strength for CFDST columns with concrete imperfections.

REFERENCES

[1] Schneider, S. P. (1998). Axially loaded concrete-filled steel tubes. Journal of structural engineering, 124(10), pp. 1125-1138. DOI: 10.1061/(ASCE)0733-9445(1998)124:10(1125).

[2] Varma, A. H., Ricles, J. M., Sause, R. and Lu L.W. (2002). Experimental behavior of high strength square concrete-filled steel tube beam-columns. Journal of structural engineering, 128(3), pp. 309-318. DOI: 10.1061/ASCE0733-94452002128:3309.

[3] Tao, Z., Han, L.-H. and Zhao, X.-L. (2004). Behaviour of concrete-filled double skin (CHS Inner and CHS Outer) steel tubular stub columns and beam-columns. Journal of Construction Steel Research, 60(8), pp. 1129-1158. DOI: 10.1016/j.jcsr.2003.11.008.

[4] Wang, J., Cheng, A., Shen, Q., Li, G. and Xiao, Q. (2022). Eccentric compression behaviour and assessment of CFET short columns offering spherical-cap gaps. Journal of Construction Steel Research, 197, 107476. DOI: 10.1016/j.jcsr.2022.107476.

[5] Elchalakani, M., Zhao, X.-L. and Grzebieta, R. (2002). Tests on concrete filled double-skin (CHS outer and SHS inner) composite short columns under axial compression, Thin-Walled Structures, 40, pp. 415-441. DOI: 10.1016/S0263-8231(02)00009-5.

[6] Uenaka, K. (2016). CFDST stub columns having outer circular and inner square sections under compression, Journal of Constructional Steel Research, 120, pp. 1-7. DOI: 10.1016/j.jcsr.2015.12.005.

[7] Ahmed M. Liang, Q. Q., Patel, V. I. and Hadi, M. N. S. (2019). Behavior of eccentrically loaded double circular steel tubular short columns filled with concrete. Engineering Structures, 201, 109790. DOI: 10.1016/j.engstruct.2019.109790.
[8] Phan, D.H.H., Patel, V.I., Liang, Q.Q., Al Abadi, H., Thai, H.-T. (2022). Numerical investigations of circular double-skin steel tubular slender beam-columns filled with ultra-high-strength concrete. Engineering Structures, 254, 113814. DOI: 10.1016/j.engstruct.2021.113814.
[9] Liao, F.-Y., Han, L.-H., He, S.-H. (2011). Behavior of CFST short column and beam with initial concrete imperfection: Experiments. Journal of Construction Steel Research, 67, pp. 1922–1935. DOI: 10.1016/j.jcsr.2011.06.009.
[10] Liao, F.-Y., Han, L.-H., Tao, Z. (2013). Behaviour of CFST stub columns with initial concrete imperfection: Analysis and calculations. Thin-Walled Structures, 70, pp. 57–69. DOI: 10.1016/j.tws.2013.04.012.
[11] Hu, H.-S., Huang, N.-J., Basha, S.H., Deng, Y.-P., Tan, Y.-Y, Wang, J.-B. (2024). Structural performance of circular CFST columns with circumferential gap imperfections. Journal of Construction Steel Research, 218, 108714. DOI: 10.1016/j.jcsr.2024.108714.
[12] Kumar, M. (2024). Effect of imperfection on behaviour of axial loaded square and rectangular concrete-filled steel tubular columns. Structures, 60, 105931. DOI: 10.1016/j.istruc.2024.105931.
[13] Shao, Z., Zha, X., Deng, J. (2024). Study on the axial compressive capacity of CFST columns with gap defects. Structures, 66, 106882. DOI: 10.1016/j.istruc.2024.106882.
[14] Shen, Q., Wang, J., Wang, F., Li, G., Hu, Z. (2022). Axial loading mechanism analyses and evaluation methods of CCFT short columns with gap defects. Structures, 46, pp.1422–1432. DOI: 10.1016/j.istruc.2022.11.015.
[15] Siguerdjidjene, H., Houari, A., Madani, K., Amroune, S., Mokhtari, M., Mohamad, B. (2024). Predicting damage in notched functionally graded materials plates through extended finite element method based on computational simulations. Frattura ed Integrità Strutturale, 18. pp. 1–23. DOI: 10.3221/IGF-ESIS.70.01.
[16] Shen, Q., Li, J., Wang, J. (2022). Experimental, numerical and design investigations on the performance of axially-loaded ECFT stub columns with spherical-cap gaps. Structures, 46, pp. 109–127. DOI: 10.1016/j.istruc.2022.10.022.
[17] Dai P, Liao F, Hou C, Yang Y, Wang R. (2023). Performance of concrete filled steel tubular (CFST) members with circumferential gap under lateral impact. Journal of Construction Steel Research, 210, 108103. DOI: 10.1016/j.jcsr.2023.108103.
[18] de Macêdo Wahrhaftig, A., Plevris, V., Abdullah Mohamad, B., Lopes Pereira, D. (2023). Minimum design bending moment for systems of equivalent stiffness. Structures, 57, 105224. DOI: 10.1016/j.istruc.2023.105224.
[19] EN 1994-1-1 (EC-4) (2004). Design of composite steel and concrete structures, part 1-1, general rules and rules for building. Commission of European Communities.
[20] Pagoulatou, M., Sheehan, T., Dai, X.H., Lam, D. (2014). Finite element analysis on the capacity of circular concrete-filled double-skin steel tubular (CFDST) stub columns. Engineering Structures, 72, pp. 102–112. DOI: 10.1016/j.engstruct.2014.04.039.
[21] IS 516 (Part 1/Sec 1) (2021). Hardened concrete methods of test part 1 testing of strength of hardened concrete section 1 compressive, flexural and split tensile strength. New Delhi, Bureau of Indian Standards.
[22] IS 10262 (2019). Recommended guidelines for concrete mix design. New Delhi, Bureau of Indian Standards.
[23] IS 1608 (2005). Metallic materials - Tensile testing at ambient temperature, New Delhi, Bureau of Indian Standards.
[24] Patel, A.J., Purohit, S.P. (2023). Axial-flexural behaviour of concrete filled double skinned steel tubular (CFDST) composite column: Experimental investigations. Materials Today Proceedings. DOI: 10.1016/j.matpr.2023.03.719.
[25] Garg, V., Patel, A.J., Purohit, S. (2022). Experimental Investigations on Axial–Flexural Behaviour of Slender Concrete Filled Steel Tubular Columns. Journal of The Institution of Engineers (India): Series A, 103, pp. 1089–1100. DOI: 10.1007/s40030-022-00670-0.
[26] Han, L.-H., Zhao, X.-L., Tao, Z. (2001). Tests and mechanics model for concrete-filled SHS stub columns, columns and beam-columns. Steel and Composite Structures, 1, pp. 51–74. DOI: 10.12989/scs.2001.1.1.051.
[27] Han, L.-H., Huang, H., Zhao, X.-L. (2009). Analytical behaviour of concrete-filled double skin steel tubular (CFDST) beam-columns under cyclic loading. Thin-Walled Structures, 47, pp. 668–680. DOI: 10.1016/j.tws.2008.11.008.